

# EXTRUSION-BASED ADDITIVE MANUFACTURING OF THE MOISTURE-CURED SILICONE ELASTOMER

Y. Jin,\* †, J. Plott†, A. J. Shih†

\* Department of Mechanical Engineering, Zhejiang University, Hangzhou, China 310027

† Department of Mechanical Engineering, The University of Michigan, Ann Arbor, MI 48105

REVIEWED

## Abstract

The extrusion-based additive manufacturing (AM) of moisture-cured silicone elastomer for complex freeform shape is studied. Due to its low elastic modulus and poor shape retaining ability during the layer-by-layer process, silicone elastomer AM is technically challenging. The experiment for extrusion of room temperature vulcanization silicone elastomer is conducted to study effects of air pressure, nozzle size and speed, layer height and distance between silicone lines on the flow rate and cross-sectional geometry of silicone elastomer AM. The COMSOL™ Multiphysics simulation using the level function to track the silicone-air interface is applied to model the silicone flow. Modeling and experimental results of the diameter and flow rate of silicone under the free flowing condition has good agreement and shows the potential for model-based guidelines for AM of silicone elastomers. Effects of the nozzle speed, layer height, and distance between two adjacent lines are investigated and demonstrate the feasibility and limitations of AM of silicone elastomer.

## Nomenclature

|          |  |
|----------|--|
| $a$      | Long radius of the cross-section of extruded silicone  |
| $b$      | Short radius of the cross-section of extruded silicone |
| $c$      | Distance between two adjacent silicone lines           |
| $d$      | Diameter of extruded silicone                          |
| $d_i$    | Inner diameter (ID) of nozzle tip                      |
| $d_o$    | Outer diameter (OD) of nozzle tip                      |
| $l$      | Length of the extruded silicone                        |
| $M$      | Mass   |
| $p$      | Hydrostatic pressure                                   |
| $P$      | Air pressure inside the syringe chamber                |
| $Q$      | Flowrate   |
| $t$      | Layer height   |
| $v$      | Speed of nozzle in the XY plane                        |
| $\gamma$ | Shear rate   |
| $\rho$   | Density  |
| $\mu$    | Viscosity  |

## Introduction

Silicone elastomers are inert materials unique for their wide range of useful properties, including thermal stability, bio-compatibility, hydrophobic nature, electrical insulation, low chemical reactivity and toxicity, and resistance to ultraviolet radiation [1]. These and other properties have distinguished silicone elastomers for

many industrial applications including automotive, consumer, medical, and others. For example, in healthcare, the biocompatible and soft silicone elastomer make it ideal for maxillofacial prosthesis [2] and augmentation of soft tissue in plastic surgery [3]. Molding is currently the most common manufacturing process for silicone elastomers [4]. The mold, typically made of hardened tool steel, usually requires extensive capital cost and long lead times. Although molding is ideal for high volume mass production, the cost and lead time often limit the low volume production of custom silicone elastomer products. The ability for layer-by-layer additive manufacturing (AM) of silicone elastomer can overcome this barrier. In this study, the extrusion-based AM of moisture-cured silicone elastomers is explored to directly create the 3D freeform shape of silicone elastomer.

Extrusion-based AM is a process whereby the viscous material is extruded through a nozzle for line-by-line building of a layer in an object [5]. Computer-controlled motion stages are used to control the movement of the nozzle for material deposition. There are two approaches for extrusion-based AM of silicone elastomer. The first is to use moisture-cured room temperature vulcanization (RTV) silicone elastomer, which is cured at the room temperature after extrusion from the nozzle. Another approach is to mix two types of silicone (commonly known as A and B) and then extrude the mixture out of the nozzle for AM. The advantage of moisture-cured silicone elastomer AM is the simplicity and flexibility to fabricate soft freeform silicone elastomer parts. The soft silicone elastomer is targeted to have the elastic modulus of the work-material lower than 120 MPa. Most of current AM materials, including metals, ceramics, and plastics, have high elastic moduli to maintain the shape for layer-by-layer AM. When the extrusion-based AM technology is used for soft materials, many technical challenges arise. For example, the cross-sectional geometry, connection of lines and deformation of the soft silicone elastomer to achieve dimensionally accurate shapes are important topics of research.

Extrusion-based AM of soft materials has been studied for fabrication of hydrogel scaffolds with specific shape and internal interconnected porous structure [6]. Tissue engineering is another application of soft material AM. Mironov et al. [7] developed a cell printer to stack soft materials (e.g. gels, single cells and cell aggregates) to build vascular and organ structures. The Freiburg Materials Research Center has developed an extrusion-based hydrogel and polymer AM machine for tissue engineering [8]. This approach has been applied for tissue scaffolds [9], biological matrices [10], fiber membrane [11], dental devices [12], and bio-composite scaffolds [13]. However, the research in extrusion-based silicone elastomer AM is still lacking. There is also a need for numerical modeling of the silicone extrusion process to predict the air pressure required for a specific nozzle size and flow rate, all critical parameters for this extrusion-based AM process.

This research is aimed to narrow this gap by studying the extrusion-based AM of RTV moisture-cured silicone elastomer. The experimental setup is presented and the process parameters are described in the following section. A numerical simulation is developed to model the size of free flowing silicone extrusion and predict the diameter and flow rate of the silicone. Results of experiments and simulation are compared and effects of key process parameters are discussed.

## **Material and Experimental Setup**

### **Silicone material**

The silicone used in this study is the 890-SL RTV moisture-cured silicone (Dow Corning, Midland, Michigan). This is a one-part silicone elastomer that cures upon exposure to atmospheric moisture [14].

### **Experimental setup**

The experimental setup is shown in Fig. 1(a). The system consists of: (1) silicone syringe and the nozzle, (2) pressure regulator, (3) motion stages and (4) controller and data acquisition system.

The silicone in a 25mm inner diameter syringe is extruded through a nozzle tip by controlling the air pressure inside the syringe using an electronic pressure regulator (Performus™ III by Nordson, Westlake, Ohio) until a steady-state flow rate is reached. The regulator has 3.5 kPa resolution to control the silicone flow rate.

An Arduino™ Mega 2560 controller is used to regulate air pressure to adjust the extrusion flow rate and synchronize with linear motion stages. Three linear stages (Model 200cri, Siskiyou, Grants Pass, Oregon) are used to guide the motion of the extrusion nozzle in X, Y, and Z directions (Fig. 1(b)) using the motion controller (Model MC-4SA, National Aperture Inc., Salem, New Hampshire). The nozzle extrudes and builds a layer of silicone in the horizontal XY plane. After finishing a layer, the Z stage lifts the nozzle tip to build another layer. A 250mm by 250mm horizontal aluminium plate is the base surface for the first layer of silicone elastomer. A digital camera with close-up lens is used to take images of the silicone for measurement.

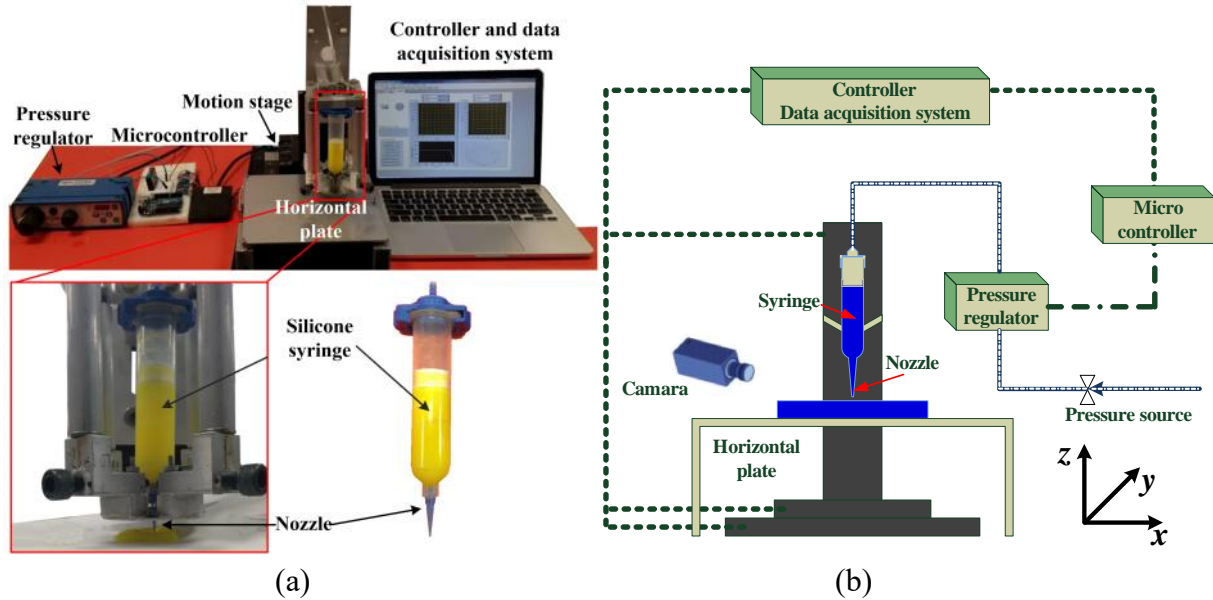


Fig.1 (a) Experimental setup and (b) scheme of the extrusion-based silicone elastomer AM system.

### Input parameters

As shown in Fig. 2, there are five key input process parameters for the extrusion-based silicone AM process.

- Inner diameter of nozzle tip ( $d_i$ ): This is the ID of the nozzle tip orifice, which determines the diameter and influence the flow rate of extruded silicone.
- Air pressure ( $P$ ): The air pressure needs to match to the nozzle ID to achieve the target flow rate for silicone extrusion.
- Nozzle speed in the XY plane ( $v$ ): The X and Y stages combine to control the nozzle speed in the XY plane to lay lines for silicone AM. The nozzle speed needs to match to the silicone flow rate.
- Layer height ( $t$ ): The layer height is the distance in the Z direction from the nozzle tip to the surface of the previous layer, as shown in the layer deposition condition in Fig. 2(a).
- Distance between two adjacent silicone lines ( $c$ ): The distance between two adjacent silicone lines, as shown in Fig. 2(c). This parameter affects the bonding and structural integrity of the silicone elastomer AM part.

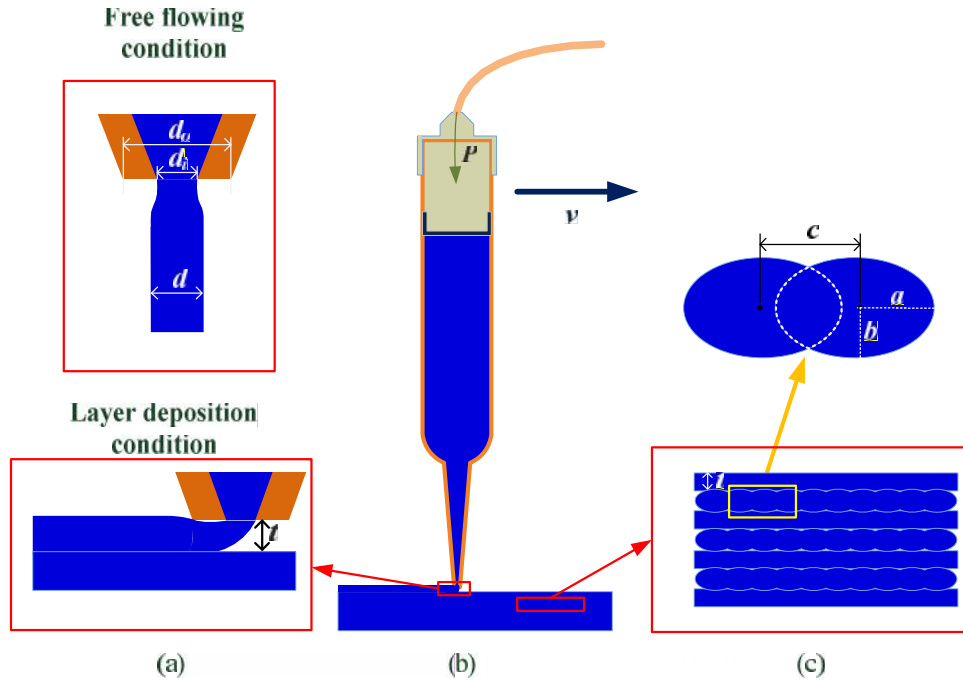


Fig. 2 Input and output parameters of silicone AM: (a) free flowing and layer deposition conditions, (b) the extrusion-based silicone AM process, and (c) cross-section view of the layers and parameters, a, b, and c.

### Output parameters and measurements

Three output process parameters are:

- Diameter of extruded silicone  $d$ : This is the diameter of silicone under the free flowing condition (Fig. 2(a)).
- Flow rate  $Q$ : This is the volumetric flow rate of the silicone under the free flow condition.
- Cross-sectional shape with long radius  $a$  and short radius  $b$ : This is the cross-section of the silicone under the layer deposition condition in Fig. 2(c).

The diameter  $d$  is measured using imaging processing technique. Fig. 3(a) shows the digital image of extruded silicone under the free flowing condition. Threshold intensity is used to process the data to either black or white pixels, as shown in Fig. 3(b). Along the Z direction, the number of black pixel is identified and plotted as in Fig. 3(c). The Z position of the nozzle tip OD (with diameter  $d_o$ ) and the steady-state extruded silicone diameter ( $d$ ) are identified and number of black pixels is denoted as  $N_{tip}$  and  $N_{silicone}$ . The extruded silicone diameter  $d$  can be calculated using:

$$d = \frac{N_{silicone}}{N_{tip}} d_o \quad (1)$$

The weight of extruding silicone under the free flow condition in a given time is measured using an electronic scale (Model HRB-103, Tree). The weight of silicone is converted to volume to calculate the flow rate.

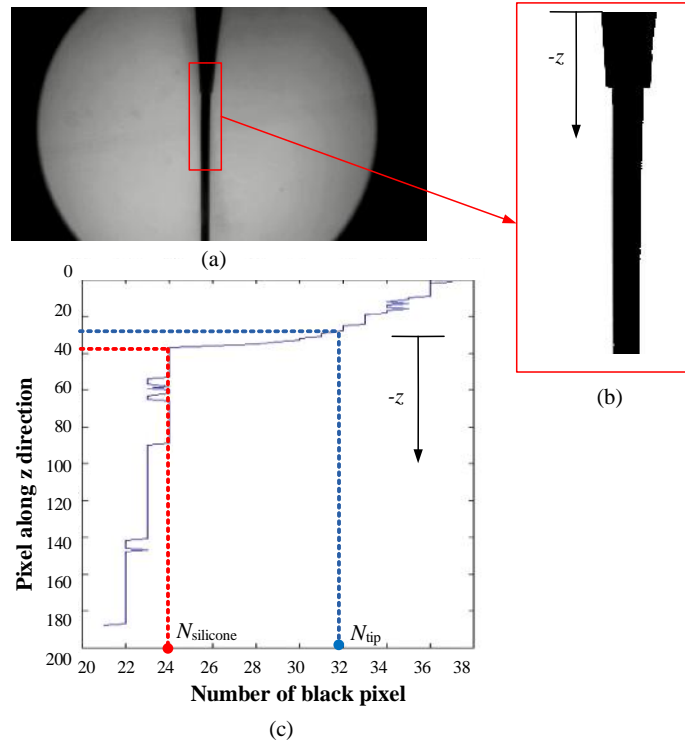


Fig. 3 Measurement of the diameter of extruded free-flowing silicone: (a) image of the camera with close-up lens, (b) pixel representation of the image, and (c) calibration of the nozzle OD and the measurement of  $d$ .

The  $a$  and  $b$  of cross section of the silicone in the layer deposition condition are measured using image processing. A sample cross-section is illustrated in Fig. 4. The elliptical profile of the cross-section of an extruded silicone elastomer line is identified to estimate parameters  $a$  and  $b$ .

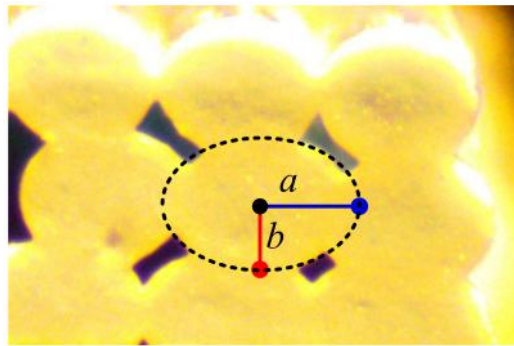


Fig.4 Cross-section of extruded silicone lines.

## Experimental Design

Five sets of experiments are designed to investigate relationships between input and output parameters during the AM of silicone elastomer.

- Exp. I – Effect of  $d_i$ : Under the free flow condition, the size  $d_i$  and the flow rate  $Q$  of the extruding silicone are affected by the nozzle orifice size  $d_i$  and air pressure  $P$ . In this study, four nozzles with  $d_i=0.41, 0.61, 0.84$  and  $1.19$  mm are tested under  $P=207$  kPa. The  $d$  and  $Q$  are measured.
- Exp. II – Effect of  $P$ : With  $d_i=0.41$  mm, the air pressure is set to be 138, 162, 207, 241, 276, 310, and 345

kPa to measure the  $d$  and  $Q$  under the free flow condition.

- Exp. III – Effect of  $v$ : Effect of the nozzle speed matching with silicone extrusion speed is investigated. The nozzle speed  $v$  is controlled to be 15, 20, 25, 30, and 35 mm/s to study the shape of silicone lines with  $t=c=0.84$  mm,  $d_i=0.41$  mm, and  $P=262$  kPa.
- Exp. IV – Effect of  $t$ : Experiments with  $t=0.5, 0.6, 0.7,$  and  $0.84$  mm are conducted with  $d_i=0.41$  mm,  $P=262$  kPa,  $v=25$  mm/s,  $c=0.84$  mm (the diameter of free flowing silicone).
- Exp. V – Effect of  $c$ : Experiments with  $c=0.5, 0.6, 0.7,$  and  $0.84$  mm are conducted with  $d_i=0.41$  mm,  $P=262$  kPa,  $v=25$  mm/s, and  $t=0.84$  mm.

### Numerical Modeling of Silicone Flow

The COMSOL™ Multiphysics (v4.4) is used to simulate the silicone extrusion process.

#### Governing equations

The silicone is modelled as an incompressible fluid with the mass conservation:

$$\nabla \cdot \mathbf{u} = 0 \quad (2)$$

where  $\mathbf{u}$  is the velocity vector of silicone.

The dynamic equilibrium of the silicone can be expressed by the momentum equation.

$$\rho \left( \frac{\partial \mathbf{u}}{\partial t} + \mathbf{u} \cdot \nabla \mathbf{u} \right) - \nabla \cdot \left( -\nabla \mathbf{u} + \nabla \mathbf{u}^T \right) + \nabla p = 0 \quad (3)$$

where  $\rho$  is the density,  $\mu$  is the viscosity, and  $p$  is the hydrostatic pressure.

The non-Newtonian Carreau model is used to describe the viscosity of silicone based on the viscosity of the silicone at infinite shear rate  $\mu_\infty$  at zero shear rate  $\mu_0$ .

$$\mu = \mu_\infty + (\mu_0 - \mu_\infty) \left[ 1 + (\dot{\gamma})^2 \right]^{\frac{n-1}{2}} \quad (4)$$

where  $\lambda$  and  $n$  are material constants. Based on the material properties provided by the material supplier (Dow Corning), these parameters are as follows:  $\mu_\infty=0$ ,  $\mu_0=62.5$  Pa·s,  $\lambda=1.73 \times 10^{-2}$  s,  $n=0.5$ , and  $\rho=1039$  kg/m<sup>3</sup>.

A laminar two-phase flow model [15] is used to simulate the silicone flow. For tracking the interface between air and silicone, the level set method [16] is applied. The level set method use a function  $\phi$  to describe the interface between the silicone and air. The value of  $\phi$  varies from 0 to 1 in a transition layer near the interface. On the interface, the value of  $\phi$  equals to 0.5. The convection of the level set function and interface between two fluids is [16].

$$\frac{\partial \phi}{\partial t} + \nabla \cdot (\phi \mathbf{u}) + \chi \left[ (\nabla \cdot (\phi (1-\phi) \frac{\nabla \phi}{|\nabla \phi|}) - \nu \nabla \cdot \nabla \phi \right] = 0 \quad (5)$$

where  $\varepsilon$  is proportional to the thickness of the convection layer and  $\gamma$  determines the amount of the reinitialization [16]. Meanwhile, the level set function can describe the smooth change of density  $\rho$  and viscosity  $\mu$  across the interface.

$$\begin{aligned} \rho &= \rho_{air} + (\rho_{silicoen} - \rho_{air}) \phi \\ \mu &= \mu_{air} + (\mu_{silicoen} - \mu_{air}) \phi \end{aligned} \quad (6)$$

#### Mesh and initial and boundary conditions

An axisymmetric model, as shown in Fig. 5, is used to represent the silicone inside the syringe chamber and the nozzle. An adaptive meshing operation is applied to model the silicone extrusion process, as illustrated in the close-up view around the nozzle tip. Boundary conditions of the silicone and air domains at stationary (zero velocity condition) are defined in Fig. 5. There are three boundary conditions, denoted as BC I, BC II and BC III. BC I is the inlet of the silicone, which is maintained at the pressure  $P$ , at the top of the syringe chamber. BC II is the no-slip condition on the syringe wall between the silicone and the control volume boundary of air. BC III is the outlet at the bottom of the air control volume with 101.3 kPa. The interface between the silicone and air at the start of the simulation is assumed at the nozzle tip.

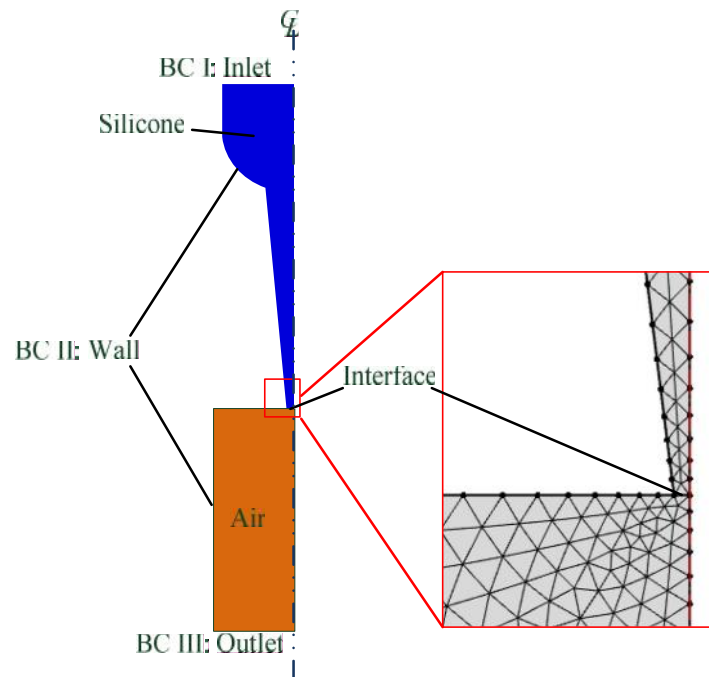


Fig. 5 Boundary conditions of the axisymmetric model at the start of simulation.

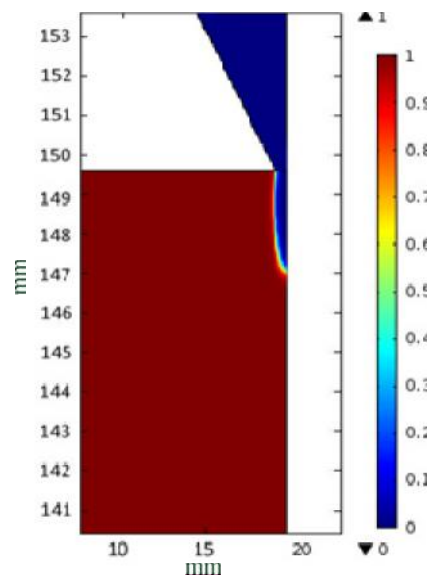


Fig. 6 The value of  $\phi$  of level set function for free flowing silicone.

## Results and discussions

### Results of EXP. I

Fig. 6 is the value of  $\varphi$  for silicone extruded through the nozzle in steady-state free flowing condition. The interface between the silicone and air is determined with  $\varphi=0.5$ . The diameter,  $d$ , of the extruded silicone is slightly expanded after extrusion from the nozzle orifice. Due to the gravity effect, the diameter of silicone is reduced. The largest diameter of the silicone out of the nozzle is identified and used for parameter  $d$ , presented in Fig. 7.

Fig. 7 shows good agreement between the experimentally measured and numerically predicted  $d$  under free flowing condition in Exp. I with  $d_i=0.41, 0.61, 0.84$  and  $1.19$  mm. The  $d$  is about 10 to 15% larger than  $d_i$ .

The model predicted and experimental measured  $Q$  also has a good agreement. Higher  $d_i$  corresponds to a larger area of the nozzle orifice and the quadratic increase in the  $Q$ .

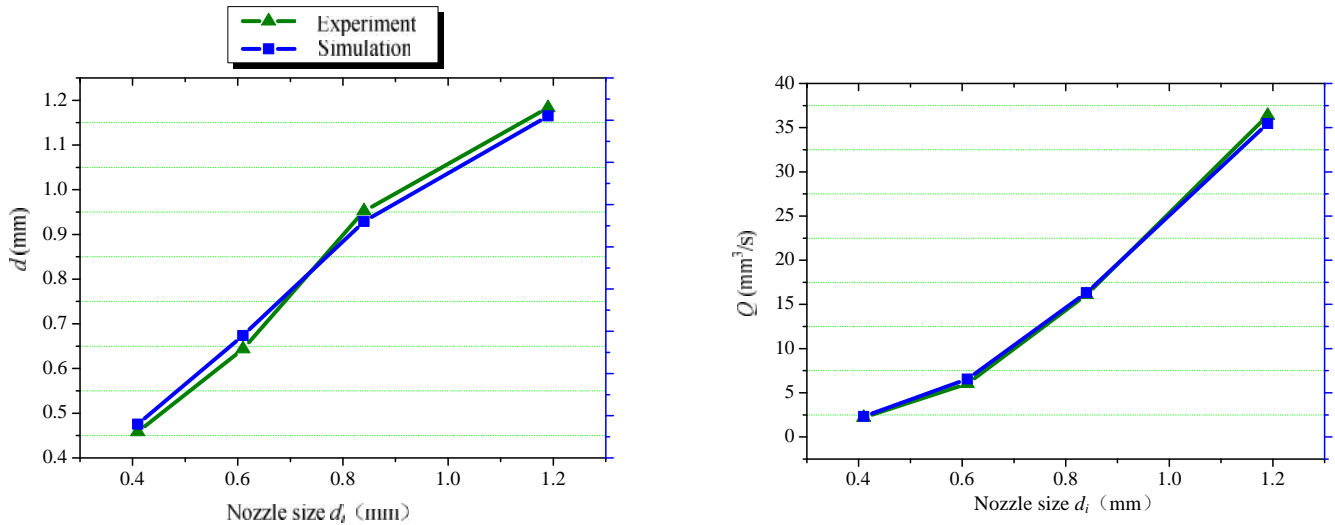


Fig. 7 Experimental and modeling results of  $d$  and  $Q$  vs.  $d_i$  in Exp. I.

## Results of EXP. II

Fig. 8 shows the inverse relationship between  $P$  and  $d$ , which is validated by both experimental measurement and numerical simulation for  $P = 138, 162, 207, 241, 276, 310,$  and  $345$  kPa. Under low  $P$  (138kPa), the silicone expands and the diameter  $d$  is 0.55 mm, much larger than the 0.41 mm  $d_i$ . The  $d$  is reduced to slightly lower than  $d_i$  at the highest pressure (345 kPa). As expected, the  $Q$  increases at a higher  $P$ , as shown in Fig. 8.

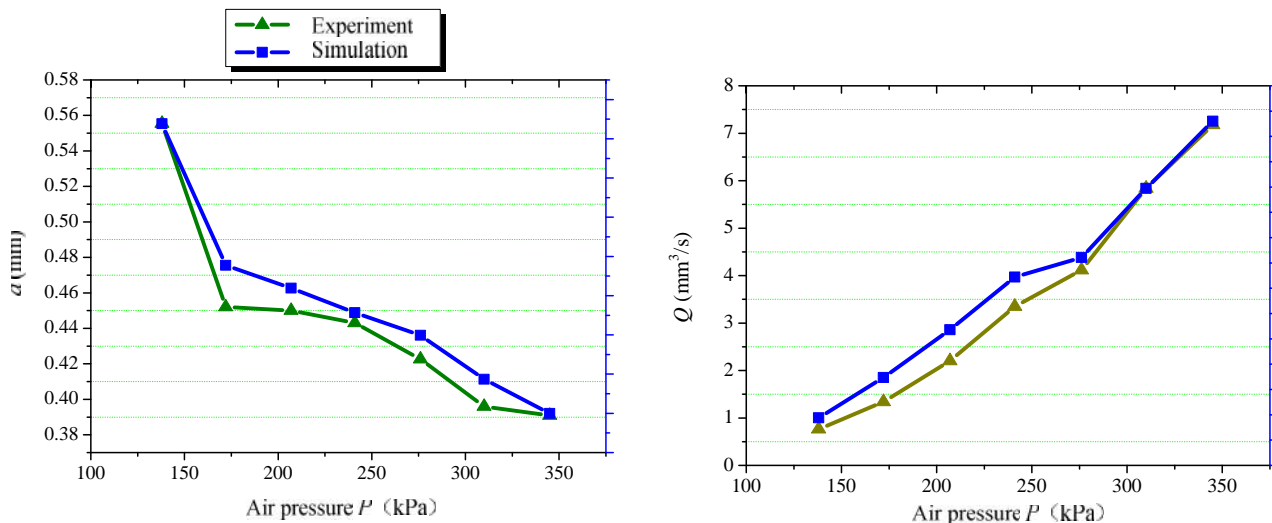


Fig.8 Experimental and modeling results of  $d$  and  $Q$  vs.  $P$  in Exp. II.

The agreement between experiment measured and model predicted  $d$  and  $Q$  in Fig. 8 is also reasonable.

Good agreement between the experimental and modelling results in Figs. 7 and 8 validates the approach using level set function for modelling of the silicone flow for extrusion-based AM.

### Results of Exp. III

The picture of the silicone lines for  $v = 15, 20, 25, 30,$  and  $35$  mm/s in Exp. III is shown in Fig. 9. Results of the long and short radii of the cross section are provided in Table 1. Under the given  $Q = 3.6$  mm<sup>3</sup>/s, at the highest  $v$  (35 mm/s), the silicone line is discontinuous. At a lower  $v$ , the silicone line becomes wider. The silicone elastomer can be stretched or compressed to a certain range. Under a given extrusion flow rate,  $v$  can vary within a range for extrusion-based AM.

Table 1 Cross section with different nozzle speed

| Nozzle speed $v$<br>(mm/s) | 15                      | 20                 | 25                   | 30                   | 35                      |
|----------------------------|-------------------------|--------------------|----------------------|----------------------|-------------------------|
| Long radius $a$<br>(mm)    | 1.015                   | 0.645              | 0.42                 | 0.36                 | 0.265                   |
| Short radius $b$<br>(mm)   | 0.425                   | 0.425              | 0.42                 | 0.415                | 0.405                   |
| Cross section              | Continuous<br>Very wide | Continuous<br>Wide | Continuous<br>Normal | Continuous<br>narrow | Crack<br>Very<br>narrow |

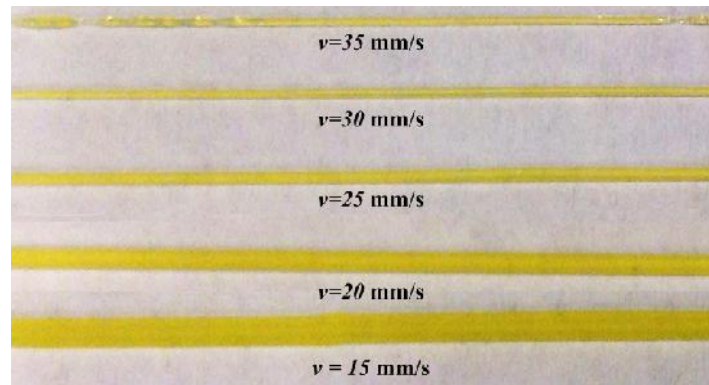


Fig. 9 The silicone elastomer line vs. nozzle speed  $v$  in Exp.III.

### Results of Exp. IV

The  $a$ ,  $b$ , and the cross-section views of AM silicone elastomer lines for  $t = 0.5, 0.6, 0.7,$  to  $0.84$  mm in Exp. IV are shown in Fig. 10. As expected, a lower  $t$  compresses the silicone after extrusion, increases  $a$ , and decreases  $b$ . The  $b$  is about half of the  $t$  due to compression of the silicone between the nozzle and the layer surface. The layer height  $t$  influences the silicone elastomer AM accuracy and efficiency. If  $t$  is large, the silicone elastomer AM is more efficient as the number of layers decreases, while the accuracy of prints is compromised. A balance is required in terms of  $t$ . As  $t$  increases while  $c$  remains the same, the cross section turns from an ellipse to a circle and  $a$  becomes smaller.

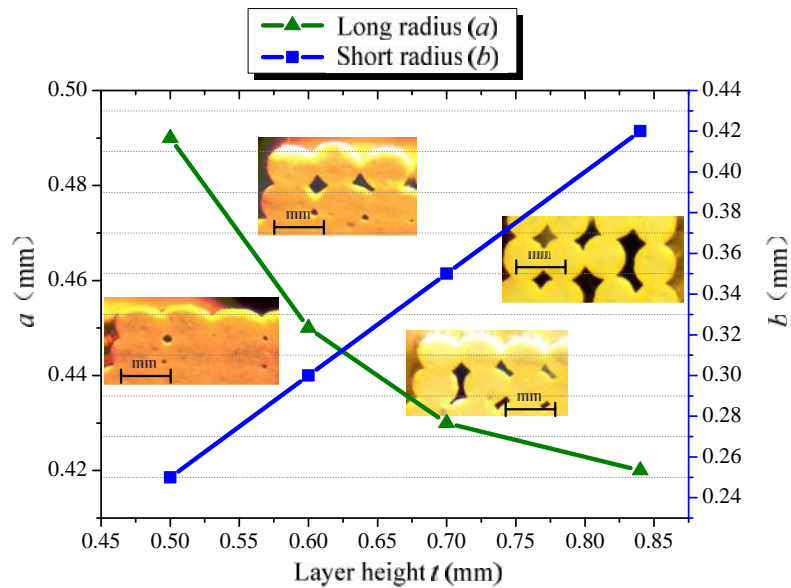


Fig. 10 Cross section vs. layer height  $t$

### Results of Exp. V

The  $a$ ,  $b$ , and the cross-section view of AM silicone elastomer lines for  $c = 0.5, 0.6, 0.7, 0.84$  mm in Exp. V are shown in Fig. 11. The  $b$  is about 0.42 mm, half of the  $t$ . Under a narrow (low)  $c$ , the  $a$  is lower due to the squeezing between lines. The  $c$  affects the bonding strength of silicone lines and structural integrity of AM silicone elastomer parts. A larger  $c$  could be used for internal structure, while a narrower  $c$  may be better for surfaces.

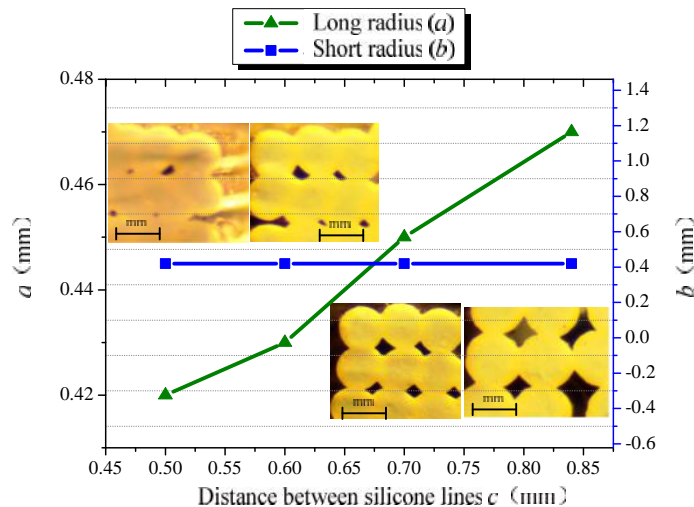


Fig. 11 Cross section vs. distance between silicone lines  $c$

### Conclusions

This research demonstrated the feasibility of extrusion-based AM of silicone elastomers and systematically investigated effects of five input parameters on the shape and flow rate under both free flowing and layer deposition conditions. The Comsol<sup>TM</sup> multiphysics modelling with level function to predict the silicone-air interface had also proven to be feasible to simulate the silicone flow during the extrusion process. This paper presented some initial but fundamental and quantitative investigations on the silicone elastomer AM process. The mechanical properties of the AM silicone elastomer parts will be further studied in our future study.

## Acknowledgements

We acknowledge the support from Dow Corning.

## References

- [1] Moretto H, Schulze M, Wagner G, Silicones BE, Hawkins S, Russey W, Schulz G (1993) Ullmann's Encyclopedia of Industrial Chemistry, in, Verlag Chemie: Weinheim, Germany.
- [2] França DCC, De Castro AL, Soubhia AMP, Tucci R, Goiato MC. Biocompatibility evaluation of 3 facial silicone elastomers. *Journal of Craniofacial Surgery*; 2011. 22(3): 837-840.
- [3] Chasan PE. The history of injectable silicone fluids for soft-tissue augmentation. *Plastic and reconstructive surgery*; 2007. 120(7): 2034-2040.
- [4] Saour S, Shaaban H, Mcphail J, Mcarthur P. Customised silicone prostheses for the reconstruction of chest wall defects: technique of manufacture and final outcome. *Journal of Plastic, Reconstructive & Aesthetic Surgery*; 2008. 61(10): 1205-1209.
- [5] Hoque ME, Chuan YL, Pashby I. Extrusion based rapid prototyping technique: an advanced platform for tissue engineering scaffold fabrication. *Biopolymers*; 2012. 97(2): 83-93.
- [6] Landers R, Pfister A, Hübner U, John H, Schmelzeisen R, Mülhaupt R. Fabrication of soft tissue engineering scaffolds by means of rapid prototyping techniques. *Journal of materials science*; 2002. 37(15): 3107-3116.
- [7] Mironov V, Boland T, Trusk T, Forgacs G, Markwald RR. Organ printing: computer-aided jet-based 3D tissue engineering. *Trends in Biotechnology*; 2003. 21(4): 157-161.
- [8] Carvalho C, Landers R, Mülhaupt R. Soft and hard implant fabrication using 3D-Biplotting™.
- [9] Rücker M, Laschke MW, Junker D, Carvalho C, Tavassol F, Mülhaupt R, Gellrich NC, Menger MD. Vascularization and biocompatibility of scaffolds consisting of different calcium phosphate compounds. *Journal of Biomedical Materials Research Part A*; 2008. 86(4): 1002-1011.
- [10] Maher P, Keatch R, Donnelly K, Mackay R, Paxton J. Construction of 3D biological matrices using rapid prototyping technology. *Rapid Prototyping Journal*; 2009. 15(3): 204-210.
- [11] Bettahalli N, Vicente J, Moroni L, Higuera G, Van Blitterswijk C, Wessling M, Stamatialis D. Integration of hollow fiber membranes improves nutrient supply in three-dimensional tissue constructs. *Acta Biomaterialia*; 2011. 7(9): 3312-3324.
- [12] Van Noort R. The future of dental devices is digital. *Dental Materials*; 2012. 28(1): 3-12.
- [13] Jiang C-P, Chen Y-Y. Biofabrication of hybrid bone scaffolds using a dual-nozzle bioplotter and in-vitro study of osteoblast cell. *International Journal of Precision Engineering and Manufacturing*; 2014. 15(9): 1947-1953.
- [14] Dow Corning 890-SL Silicone Joint Sealant. [cited 2012; Available from: [http://www.bondedmaterials.net/assets/data/dow\\_corning\\_890sl.pdf](http://www.bondedmaterials.net/assets/data/dow_corning_890sl.pdf).
- [15] Yue P, Feng JJ, Liu C, Shen J. A diffuse-interface method for simulating two-phase flows of complex fluids. *Journal of Fluid Mechanics*; 2004. 515: 293-317.
- [16] Olsson E, Kreiss G. A conservative level set method for two phase flow. *Journal of computational physics*; 2005. 210(1): 225-246.